PAPER
Nguyen Thi Kim Thanh *et al.*
Protection of *Shewanella oneidensis* MR-1 by manganese
ferrite nanoparticles during chromate bio-reduction

PAPER

Check for updates

Protection of *Shewanella oneidensis* MR-1 by manganese ferrite nanoparticles during chromate bio-reduction†

Diana S. Raie, (iD) [ab] Ioannis Tsonas,[c] Stefanos Mourdikoudis, (iD) [ab] Evangelia Delli, (iD) [d] Antonios Makridis, (iD) [d] Lena Ciric[e] and Nguyen Thi Kim Thanh (iD) *[ab]

Shewanella oneidensis (*S. oneidensis*) MR-1 is a metal-reducing bacterium that can bio-reduce the carcinogenic hexavalent chromium (Cr^{6+}) to a less toxic trivalent form (Cr^{3+}). The bacteriocidal effect of Cr^{6+} challenges the above bio-reduction process. This work aims to illustrate the protective role of manganese ferrite nanoparticles ($Mn_{0.2}Fe_{2.8}O_4$ NPs) to *S. oneidensis* MR-1 bacteria during the bio-reduction of Cr^{6+}. Nanostructures were characterised by transmission electron microscopy (TEM) and X-ray diffraction (XRD). The interaction between *S. oneidensis* MR-1, Cr^{6+} and $Mn_{0.2}Fe_{2.8}O_4$ NPs was monitored by X-ray photoelectron spectroscopy (XPS), which helped to unravel the oxidation states of Cr. The XPS analysis provided key insights into the oxidation states of Mn and Fe, confirming the redox interactions facilitating Cr^{6+} reduction. $Mn_{0.2}Fe_{2.8}O_4$ NPs boosted the detoxification of the removed Cr^{6+} by 2.1 and 1.4 times compared to using *S. oneidensis* MR-1 alone and NPs alone, respectively. Scanning electron microscopy (SEM) imaging evaluated the changes in the morphology of bacterial cells. After exposure to Cr^{6+}, *S. oneidensis* MR-1 cells revealed their inability to produce nanofibers, which are electrically conductive bacterial appendages. Yet, $Mn_{0.2}Fe_{2.8}O_4$ NPs provoked the formation of bacterial nanofibers. These findings highlight the potential of $Mn_{0.2}Fe_{2.8}O_4$ NPs for enhancing the bioremediation of Cr^{6+} contaminated environments.

Environmental significance

Carcinogenic hexavalent chromium leaks from industrial sites due to improper wastewater treatment into surface and groundwater, exposing flora and fauna to danger. The metal-reducing bacterium, *Shewanella oneidensis* MR-1, can reduce Cr^{6+} into less toxic Cr^{3+}; bacteria lose their viability during treatment due to the toxicity of Cr^{6+}. The novelty of this work is the discovery of a protective role of Mn-ferrite nanoparticles to *S. oneidensis* MR-1 bacteria during Cr^{6+} bio-reduction. We show that $Mn_{0.2}Fe_{2.8}O_4$ NPs induced bacterial cell elongation and promoted nanofiber formation. Such morphological changes improve bacterial cell viability in response to the sub-lethal dose of Cr^{6+} and enhance their detoxification capability. Our findings provide a promising application of using nano-$Mn_{0.2}Fe_{2.8}O_4$ in the bioremediation of Cr^{6+}-contaminated environments.

1. Introduction

Contamination of air, soil and water with heavy metals is hazardous to human health and the environment due to their toxicity, even at low concentrations[1] as they are non-biodegradable materials.[2] The Agency for Toxic Substances and Disease Registry (ATSDR) ranked chromium (Cr) the 17th on the substance priority list among many heavy metals.[3]

Cr mainly occurs in two valence states: hexavalent (Cr^{6+}) and trivalent (Cr^{3+}). Human exposure to Cr^{6+} can cause liver damage, pulmonary congestion, oedema, skin irritation, ulcer formation,[4] neurotoxicity,[5] and carcinogenesis.[6] U.S. Environmental Protection Agency (EPA) and WHO guidelines reported a permissible limit of Cr^{6+} in drinking water of 50 ppb.[7] According to the EU drinking water directive, the regulation limit for the total Cr will be 25 μg L^{-1} by 12 January 2036.[8] Since Cr^{3+} has low mobility, limited bio-absorptivity, and lower toxicity than Cr^{6+},[9] Cr^{6+} should be reduced to Cr^{3+} for its safe removal.[10]

[a] Biophysics Group, Department of Physics and Astronomy, University College London (UCL), London, WC1E 6BT, UK.
E-mail: ntk.thanh@ucl.ac.uk; Web: https://www.ntk-thanh.co.uk
[b] UCL Healthcare Biomagnetics and Nanomaterials Laboratories, 21 Albemarle Street, London, W1S 4BS, UK
[c] UCL Electronic and Electrical Engineering, UCL, Gower Street, London, WC1E 7JE, UK
[d] Laboratory of Advanced Materials and Devices, Department of Physics, Aristotle University of Thessaloniki, 54124 Thessaloniki, Greece
[e] Healthy Infrastructure Research Group, Department of Civil, Environmental & Geomatic Engineering, UCL, Gower Street, WC1E 6BT London, UK
† Electronic supplementary information (ESI) available. See DOI: https://doi.org/10.1039/d5en00204d

This journal is © The Royal Society of Chemistry 2025

Environ. Sci.: Nano, 2025, **12**, 3035–3046 | **3035**

Bio-reduction of Cr^{6+} is a cost-effective and environmentally friendly method, attracting widespread interest.[11] Some bacteria can reduce metals, acting as terminal electron acceptors under anaerobic conditions.[12] So, metal-reducing bacteria can be used for the biotic reduction of heavy metals for detoxification purposes. Such a natural process is applicable for the biological reduction of the carcinogenic Cr^{6+} into less toxic Cr^{3+} form.[13]

Shewanella oneidensis MR-1 is a model metal-reducing bacteria for detoxifying Cr^{6+}.[14–18] *S. oneidensis* MR-1 can employ Cr^{6+} as a terminal electron acceptor under anaerobic conditions.[14,15,19] The biosafety of *S. oneidensis* MR-1 is an essential criterion for selecting bioremediation biological agents. In contrast, *Pseudomonas aeruginosa* bacteria can be used for Cr^{6+} removal but are not preferred for bioremediation because they cause diseases in humans and animals.[20,21] Yet, the lethal effect of Cr^{6+} on the microbes during their respiration limited the bioremediation of Cr^{6+}.[22]

$Mn_{0.2}Fe_{2.8}O_4$ NPs showed a higher adsorption capacity for Cr^{6+} than Fe_2O_3 NPs and other tested $Mn_xFe_{3-x}O_4$ NPs.[23] This chemical structure improved the bacterial viability and microbial detoxification of Cr^{6+}.[23] The adsorption of Cr^{6+} can limit the availability of the toxic cations to cells, which could improve their viability and bio-reduction efficiency.

Herein, to the best of our knowledge, we showed for the first time the protective role of the $Mn_{0.2}Fe_{2.8}O_4$ NPs to *S. oneidensis* MR-1 during the bio-reduction of Cr^{6+}. Raie *et al.*[23] primarily investigated the adsorption and bio-removal of Cr^{6+} using $Mn_{0.2}Fe_{2.8}O_4$ NPs and *S. oneidensis* MR-1, respectively.

This article builds upon findings by Raie *et al.*,[23] and elucidates the reduction process of Cr^{6+} using XPS. In addition, this work presents bacterial imaging to visualise morphological changes in response to Cr^{6+} and NPs, providing deeper insights into the mechanism of Cr^{6+} reduction.

XPS revealed the possible reduction of Cr^{6+} to Cr^{3+} due to its interaction with $Mn_{0.2}Fe_{2.8}O_4$ NPs. This allowed us to confirm the redox-based interaction among Cr^{6+} and $Mn_{0.2}Fe_{2.8}O_4$ NPs. In addition, SEM showed the morphological change response of *S. oneidensis* MR-1 as a coping strategy in response to the toxic Cr^{6+} in the presence of $Mn_{0.2}Fe_{2.8}O_4$ NPs. This article will advance the treatment of Cr^{6+} by demonstrating its removal, unravelling its reduction mechanism and the biological implications, thereby contributing novel insights and practical advancements to nanobiotechnology and environmental applications.

2. Materials and methods

2.1 NPs preparation and characterisation

$Mn_{0.2}Fe_{2.8}O_4$ NPs were prepared by an adapted polyol solvothermal synthetic process[24,25] at 250 °C as described in our recent work.[23] In 20 mL of tetraethylene glycol (TEG), 0.3 M of iron(III) acetylacetonate (2.1 g) and 0.1 M manganese(II) acetylacetonate (0.5 g) were added. The mixture was added into a 45 mL Teflon-lined stainless-steel autoclave after being homogenised by vortex and sonication to be placed in an oven (Memmert, model UFP400) and heated within 30 min up to 250

°C for a 6 h hold at that temperature. In polyol synthesis, metal precursors are reduced by TEG, which acts as a high-temperature capping agent, solvent, and reductant. The formed metal nuclei grow and controllably coalesce together to produce the desired particles.[26,27] The produced black dispersion underwent characterisation and functionalisation by tri-sodium citrate *via* ligand exchange.[23] A JEOL JEM 1200-EX microscope operating at an acceleration voltage of 120 kV was employed to investigate the shape and size of the produced particles. The polydispersity index (PDI) is the ratio between the standard deviation and the mean nanoparticle diameter. To determine the crystal phase and the average crystallite size, we used XRD (PANalytical XPERT PRO MPD) coupled with Co K_α radiation source (λ = 1.789 Å) and an X'Celerator detector operated at 40 kV and 40 mA. An Optima 3100 XL Perkin Elmer Inductively Coupled Plasma Atomic Emission (ICP-AES) spectrometer was employed to determine the chemical composition of $Mn_xFe_{3-x}O_4$ particles. To quantify the iron content of the functionalised NPs dispersed in water, a colorimetric phenanthroline method was applied for the acid-digested NPs using a spectrophotometer (SpectraMax M2e, Molecular Devices, UK).

2.2 Sources for bacteria of interest

A freeze-dried culture of *S. oneidensis* MR-1 (LMG 19005) was purchased from BCCM/LMG bacteria collection.

2.3 Viability of *S. oneidensis* MR-1 to $Mn_{0.2}Fe_{2.8}O_4$ NPs

The impact of $Mn_{0.2}Fe_{2.8}O_4$ NPs on the viability of the *S. oneidensis* MR-1 was assessed using Guava easyCyte® flow cytometer (Merck, UK) following a protocol previously utilised by Raie *et al.*,[23] under anaerobic conditions overnight. A homogeneous bacterial cell suspension (10 μL with OD measured at λ = 600 nm equal to 0.1) was added to 80 μL of M9 minimal salts (×2) medium, containing 20 mM sodium lactate as a sole electron source, 5 mL L^{-1} each of vitamins and minerals and pH was adjusted to 7.2 by 10 mM 4-(2-hydroxyethyl)-1-piperazineethanesulfonic acid (HEPES) buffer.[23,28] Sodium fumarate (20 mM) was used as a terminal electron acceptor.[23,28] $Mn_{0.2}Fe_{2.8}O_4$ NPs (10 μL) were added to the mixture. The tested concentrations of NPs ranged from 1–60 mg mL^{-1} with an approximate total Fe content from 0.7 mg mL^{-1} to 40.6 mg mL^{-1}.

2.4 The exposure of *S. oneidensis* MR-1 to Cr^{6+} and $Mn_{0.2}Fe_{2.8}O_4$ NPs

S. oneidensis MR-1 was exposed to Cr^{6+} and $Mn_{0.2}Fe_{2.8}O_4$ NPs individually and also in a combined way overnight, in conditions similar to that mentioned in Section 2.3. Cr^{6+} (as a terminal electron acceptor) and $Mn_{0.2}Fe_{2.8}O_4$ NPs were added to this medium with concentrations of 50 mg L^{-1} (sub-lethal dose, as reported by Raie *et al.*)[23] and 1 mg mL^{-1}, respectively.[23]

2.5 Analysis of oxidation state of Cr^{6+}, Mn^{x+}, and Fe^{y+}

The oxidation states of Mn and Fe in $Mn_{0.2}Fe_{2.8}O_4$ NPs and Cr were investigated after being incubated together or separately with *S. oneidensis* MR-1 by XPS; a Kratos Analytical AXIS Ultra^{DLD} system with aluminium X-ray source (λ_{Ka}= 1486.6 eV) was used, operated under ultra-high vacuum conditions (10^{-9} torr). The experimental curves were best fitted by combining Gaussian (70%) and Lorentzian (30%) distributions, while background subtraction was performed using the Shirley equation. A normalised peak area of each element is calculated by dividing its area by the sensitivity factor.[29] To determine the redox interaction between Cr^{6+} and $Mn_{0.2}Fe_{2.8}O_4$ NPs, we compared the normalised peak areas of Mn^{2+} to Mn^{3+}, Fe^{2+} to Fe^{3+} and Cr^{3+} to Cr^{6+} in the high-resolution Mn 2p, Fe 2p and Cr 2p spectra, respectively, while only the ratios between that peak areas of Cr^{3+} to Cr^{6+} were analysed in the case of applying bacterial cells. The relative fold increase in Cr^{6+} bio-reduction was calculated by its equivalent atomic fraction to the reference values.

2.6 Imaging bacteria by SEM

To acquire SEM images, 50 μL from the untreated or $Mn_{0.2}$-$Fe_{2.8}O_4$ NPs treated *S. oneidensis* MR-1 bacteria cell suspension were deposited on a microscope cover glass (Fisher, UK). The samples were imaged using Philips XL30 FEG SEM (FEI, Eindhoven, Netherlands), which operates at an accelerating voltage of 5 keV. Cell fixation was performed using glutaraldehyde (2.5% v/v in 0.01 M PBS) for 30 min at room temperature. Samples were washed three times in phosphate-buffered saline (PBS, 0.01 M) and dehydrated for 5 min in ethanol aqueous solutions. The concentrations of ethanol aqueous solutions were 10% v/v, 30% v/v, 50% v/v, 70% v/v, 90% v/v, 100% v/v, sequentially. A double-sided carbon tape (Agar Scientific, UK) was used to attach the glass slide with the SEM specimens onto aluminium stubs. Samples were then sputter-coated with gold–palladium at 20 mA and 1.25 kV for 90 s (Palaron E5000 sputter coater).

3. Results and discussion

3.1 Characterisation of NPs

3.1.1 Morphology of NPs.
Regarding the obtained spherical $Mn_xFe_{3-x}O_4$ NPs (Fig. 1A), our results agree with Raie *et al.*,[23] Vamvakidis *et al.*,[25] and García-Soriano *et al.*,[30] who used the polyol solvothermal technique for producing spherical Mn_xFe_{3-x}-O_4 NPs.[23,25,30] The mean size of $Mn_xFe_{3-x}O_4$ NPs is 7.4 ± 1.3 nm. The PDI is 0.18, which indicates a relatively narrow size distribution.[31] Similarities in spherical shape and small size range (approximately 7–9 nm) are attributed to the specific procedure where sole polyols were used to prepare the NPs.[23,25,30]

3.1.2 Crystal structure of NPs.
Powder XRD patterns for the prepared $Mn_xFe_{3-x}O_4$ NPs recorded at room temperature are illustrated in Fig. 1B. All the diffraction peaks show the presence of the face-centred cubic (FCC) crystal structure, while no impurity phase was observed. So, the formation of
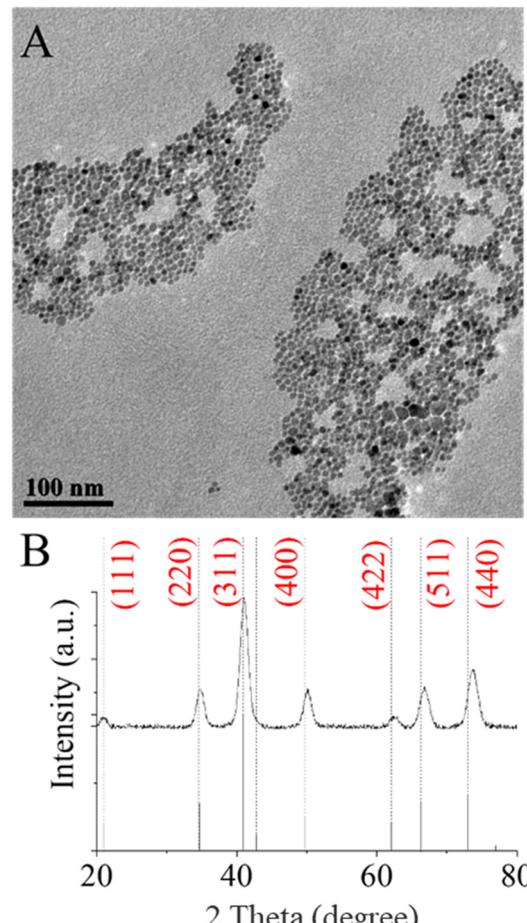

Fig. 1 $Mn_{0.2}Fe_{2.8}O_4$ NPs prepared at 250 °C for 6 h: (A) TEM images and (B) XRD patterns, and XRD reference for $MnFe_2O_4$ (PDF card no 00-010-0319).

$Mn_xFe_{3-x}O_4$ NPs was obtained through a facile polyol solvothermal process with reaction times of 6 h.

3.1.3 Elemental analysis of $Mn_xFe_{3-x}O_4$ NPs.
The formed $Mn_xFe_{3-x}O_4$ NPs have a low Mn content (x = 0.2), based on ICP-AES results. Etemadi & Plieger,[32] Oberdick *et al.*,[33] and Raie *et al.*[23] reported similar results of low Mn doping levels because $Mn(acac)_2$ is more thermally stable than $Fe(acac)_3$.[34]

3.2 Interaction of Cr^{+6} with $Mn_{0.2}Fe_{2.8}O_4$ NPs

$Mn_{0.2}Fe_{2.8}O_4$ NPs adsorbed 16.8 ± 1.6 mg g^{-1} (around 61%) of Cr^{6+}.[23] The possible reduction of the adsorbed Cr^{6+} by $Mn_{0.2}$-$Fe_{2.8}O_4$ NPs was explored here by studying the oxidation state of Mn, Fe, and Cr of the adsorbent and adsorbate by XPS, as shown in Fig. 2A.

3.2.1 Oxidation state of Mn in $Mn_{0.2}Fe_{2.8}O_4$ NPs after Cr^{6+} adsorption.
In Fig. 2B, the position of binding energy (BE) for Mn 2p was slightly shifted from 640.45 eV[23] to higher BE (641.80 eV), which could be attributed to the possible oxidation of Mn^{2+} into Mn^{3+} upon interacting with Cr^{6+}. The dissolved Mn^{3+} could generate manganese oxide (MnO_x), which provides more adsorption sites for Cr^{6+} removal.[35]
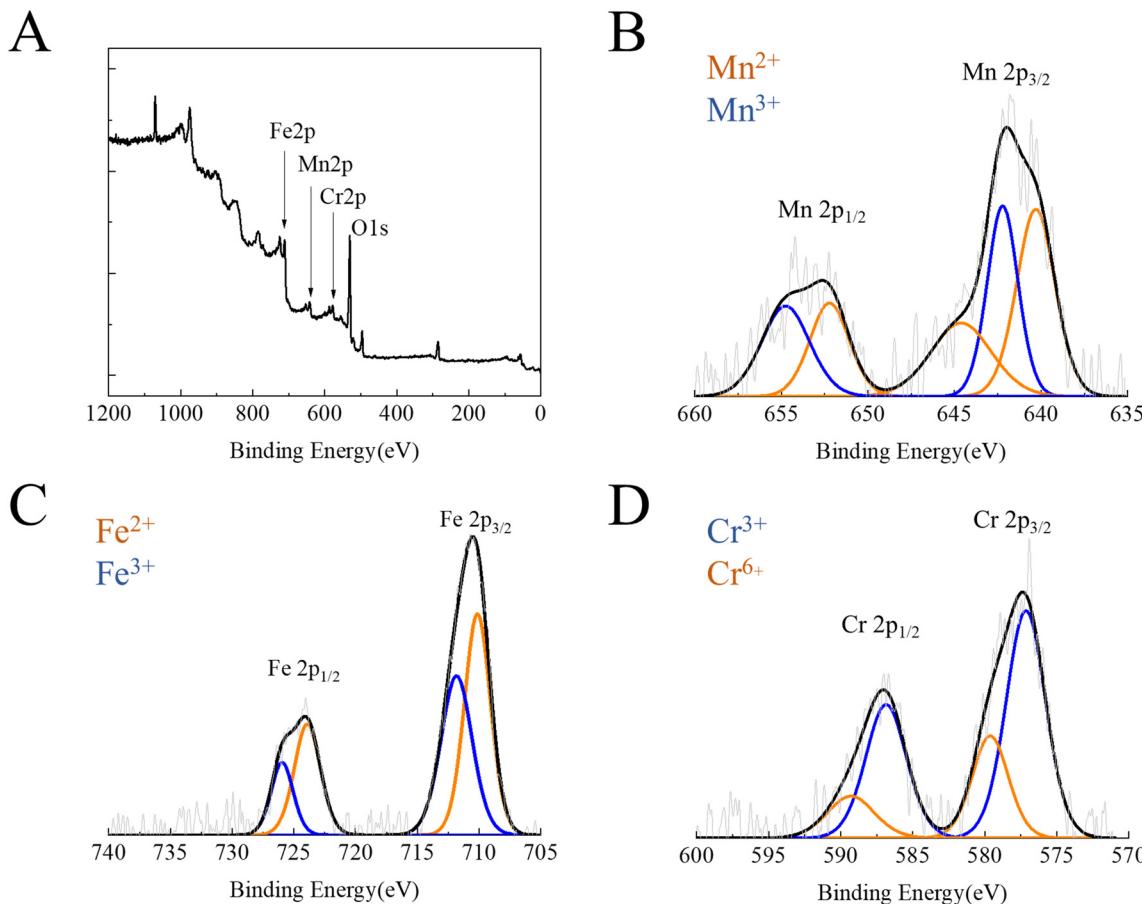
**Fig. 2** $Mn_{0.2}Fe_{2.8}O_4$ NPs treated by Cr^{6+}: (A) wide scan XPS spectrum, and high-resolution XPS spectra of (B) Mn 2p, (C) Fe 2p, and (D) Cr 2p.

In $Mn_{0.2}Fe_{2.8}O_4$ NPs,[23] Mn 2p peak, in Fig. 2B, was fitted by 5 contributions at 640.3 eV, 642.2 eV, 644.61 eV, 652.2 eV and 654.8 eV. Mn $2p_{3/2}$ was deconvoluted into 640.35 eV and 642.25 eV peaks, representing Mn^{2+} and Mn^{3+}, respectively, as shown in Fig. 2B. The peak of Mn $2p_{1/2}$ was fitted into two contributions of Mn^{2+} and Mn^{3+} at 652.15 eV and 654.6 eV, respectively.[36–39] The fifth small satellite peak at 645.2 eV was assigned to Mn^{2+} of MnO.[38] Since stoichiometric $MnFe_2O_4$ can be expressed as $MnO-Fe_2O_3$, this pointed to the formation of $Mn_xFe_{3-x}O_4$ NPs.

3.2.2 Oxidation state of Fe after Cr^{6+} interaction with $Mn_{0.2}Fe_{2.8}O_4$ NPs. After Cr^{6+} adsorption on $Mn_{0.2}Fe_{2.8}O_4$ NPs, XPS (in Fig. 2C) showed the position of BE for Fe 2p at 711 eV. A peak of Fe $2p_{3/2}$ was spotted at 710.75 eV, and the asymmetric peaks are situated at 723.9 eV, attributed to $2p_{1/2}$.[39,40] The observed signals at these BE positions probably correspond to the formation of iron oxide phase, *i.e.*, hematite or maghemite phase.[41] Unlike untreated $Mn_{0.2}Fe_{2.8}O_4$ NPs,[23] Fe 2p missed the satellite peak at 718 eV as shown in Fig. 2C, which was due to the presence of Fe_3O_4.[40] The ratio between Mn and Fe was doubled from 0.24 to 0.44 (as was reported by XPS and range based on elemental analysis by ICP in our recent work) compared to untreated $Mn_{0.2}Fe_{2.8}O_4$ NPs,[23] which can be ascribed to the release of iron in the medium.

3.2.3 Reduction of Cr^{6+} by $Mn_{0.2}Fe_{2.8}O_4$. In Fig. 2D, XPS spectra of Cr 2p showed two different peaks, corresponding to the Cr $2p_{3/2}$ (576.0 eV–578.0 eV) and Cr $2p_{1/2}$ (585.0 eV–587.0 eV) orbits. After fitting peaks with the use of the Gauss–Lorentz algorithm, two peaks arised with the BE of 577 eV relating to Cr^{3+} $2p_{3/2}$ and 586 eV belonging to Cr^{3+} $2p_{1/2}$,[42,43] which mainly corresponds to the precipitation of insoluble Cr^{3+} species, $Cr(OH)_3$ and Cr_2O_3. The adsorbed $[CrO_4]^{2-}$ on NPs[37] explained the presence of peaks at BE of 579.6 eV and 589 eV, representing Cr^{6+} $2p_{3/2}$ and $2p_{1/2}$, respectively.[43] The ratio of $[Cr^{3+}]/[Cr^{6+}]$ was estimated to be equal to 2.56. Our results point out a significant finding: the interaction between Cr^{6+} and $Mn_{0.2}Fe_{2.8}O_4$ NPs involved a redox reaction in addition to what was stated in our recent work regarding adsorption.[23] Raie *et al.* reported that the oxidation state of Mn in $Mn_{0.2}Fe_{2.8}O_4$ was mainly Mn^{2+} with a minor fraction of Mn^{4+}, and that of Fe was a mixture of Fe^{2+} and Fe^{3+}.[23] In the present study, the possible oxidation of Mn^{2+} to Mn^{3+} and Fe^{2+} to Fe^{3+}, besides the iron release, is due to the redox reaction between $Mn_{0.2}Fe_{2.8}O_4$ NPs and Cr^{6+}. The absence of Mn^{4+} XPS related peak after interaction with Cr^{6+} was attributed to the ability of Fe^{2+} to reduce Mn^{4+}, yielding Fe^{3+} and Mn^{2+}.[44] In addition to being a stabilising agent, citrate can act as a chelating agent[45] and as a reductant for Cr^{6+},[46] due to its ability to donate electrons through ligand–metal electron transfer.[46] Mn^{2+} catalyses the reduction reaction.[47]

3038 | *Environ. Sci.: Nano*, 2025, **12**, 3035–3046

This journal is © The Royal Society of Chemistry 2025

3.3 $Mn_{0.2}Fe_{2.8}O_4$ NP-assisted bacterial respiration of Cr^{6+}

S. oneidensis MR-1 can respire Cr^{6+} under anaerobic conditions.[48–50] The adsorption of Cr^{6+} (9 ± 1.5 mg g^{-1}, *i.e.* $30 \pm 0.5\%$ of removal) by $Mn_{0.2}Fe_{2.8}O_4$ NPs supported microbial survival in media supplemented by the tested *S. oneidensis* MR-1.[23] The mechanism of bio-removal of Cr^{6+} can be attributed to the respiration of Cr^{6+} into Cr^{3+} (ref. 48–50) or bio-sorption[51,52] by bacterial cells. Examining the oxidation state of Cr element *via* XPS analysis determines the interaction between Cr^{6+}, $Mn_{0.2}$-$Fe_{2.8}O_4$ NPs and *S. oneidensis* MR-1, as illustrated in Fig. 3, which positively related to the enhanced Cr^{6+} bio-reduction by 2.7–3.6 fold.[23] The reported significant drop in the XPS revealed the presence of peaks related to both Cr^{6+} and Cr^{3+} after exposing *S. oneidensis* MR-1 to Cr^{6+}.

Peaks of Cr 2p XPS were observed at BE 576.7 eV and 585.9 eV, which were related to Cr^{3+}, while peaks at 579.2 eV and 588.6 eV were assigned to Cr^{6+}, as presented in Fig. 3A. *S. oneidensis* MR-1 can reduce Cr^{6+} into Cr^{3+}, as confirmed by our XPS results in Fig. 3A and supported by the literature.[48,53]

Our findings reveal an extracellular interaction between Cr^{6+} and *S. oneidensis* MR-1 bacteria. A portion of Cr^{6+} was reduced to Cr^{3+}, resulting in a $[Cr^{3+}]/[Cr^{6+}]$ ratio of 1.7, while the remaining 41% of Cr^{6+} is adsorbed on the bacterial cell surface. The extracellular reduction of Cr^{6+} can occur *via* direct contact of Cr^{6+} with the metal-reducing protein complex on the cell surface and nanofiber. Also, *S. oneidensis* MR-1 can produce electron shuttles to promote mediated electron transfer between the cell and Cr^{6+}. *S. oneidensis* MR-1 can uptake Cr^{6+} to be reduced inside the cell to Cr^{3+}, but our results could not confirm the intracellular reduction of Cr^{6+} due to the depth limitation of XPS (7–10 nm).

Our XPS results revealed peaks related to both Cr^{6+} and Cr^{3+} after being incubated with *S. oneidensis* MR-1 in the presence of $Mn_{0.2}Fe_{2.8}O_4$ NPs. Peaks of Cr 2p XPS observed at BE 576.7 eV and 585.9 eV denote the presence of Cr^{3+}. Cr^{6+} is represented by one peak at 579.2 eV,[38] as illustrated in Fig. 3B. Similar results were reported due to using Cr^{6+} as a terminal electron acceptor during the respiration process of *S. oneidensis* MR-1.[48,53] The ratio between extracellular Cr^{3+} and Cr^{6+} was equal to 3.5. Bacteria can reduce Fe^{3+} to Fe^{2+}, and biogenic Fe^{2+} can detoxify Cr^{6+} to Cr^{3+}.[54,55] The affinity of $MnFe_2O_4$ NPs to proteins on the bacterial outer membrane can improve the contact area between a single bacterium and Cr^{6+} as an external electron acceptor.[56–59]
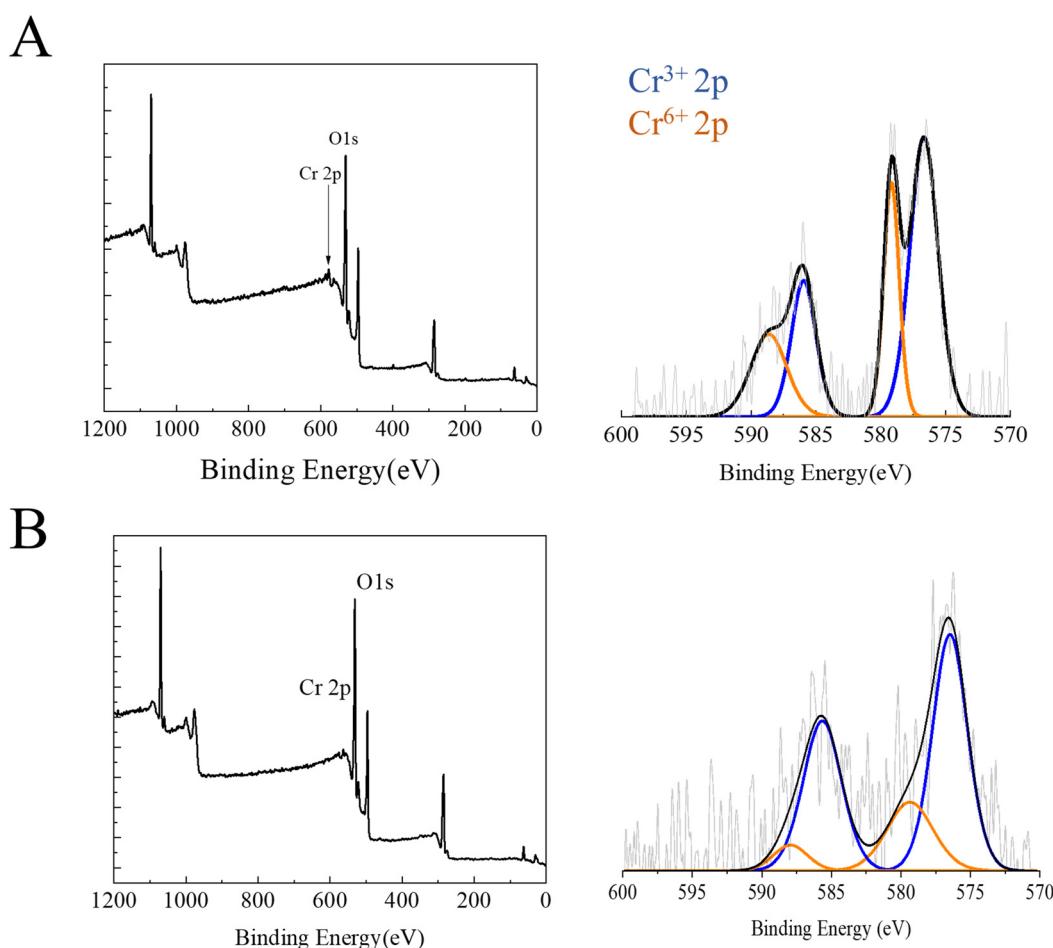

Fig. 3 Wide scan and high-resolution XPS spectra of (A) Cr 2p treated by *S. oneidensis* MR-1 alone, (B) Cr 2p after incubation of *S. oneidensis* MR-1 and $Mn_{0.2}Fe_{2.8}O_4$ NPs.

This journal is © The Royal Society of Chemistry 2025

Environ. Sci.: Nano, 2025, **12**, 3035–3046 | **3039**

In this work, the presence of both *S. oneidensis* MR-1 and $Mn_{0.2}Fe_{2.8}O_4$ NPs removed Cr^{6+} 1.37 times more than using the NPs alone. Some possible scenarios could explain how NPs enhanced the bio-reduction of *S. oneidensis* MR-1 from Cr^{6+} to Cr^{3+}. By adsorption, NPs can bridge the bacterial cell and Cr^{6+} to promote electron transfer. Cr^{6+} is adsorbed onto the $MnFe_2O_4$ NPs *via* partial chemisorption[60,61] and partial physisorption.[37] The Mn in $MnFe_2O_4$ can interact *via* ionic bonding with the O atoms of $HCrO_4^-/CrO_4^{2-}$, facilitating Cr^{6+} adsorption.[60,61] Mn^{2+} can reduce Cr^{6+} to Cr^{3+} and be oxidised to Mn^{3+}. The disproportionation of oxidised Mn^{3+} produced Mn^{2+}, causing Mn^{2+} to continue participating in the Cr^{6+} reduction. Cr^{3+} is deposited on the $MnFe_2O_4$ surface as $Cr(OH)_3$ colloids.[60,61]

The limited availability of adsorbed Cr^{6+} improved the efficiency of microbial respiration,[48,54] as was indicated by our results. Since $MnFe_2O_4$ NPs have electrochemical properties,[59,62] metal oxides can link *S. oneidensis* MR-1 with Cr^{6+} to promote direct electron transfer and act as an electron mediator from the cell to Cr^{6+}, a terminal electron acceptor.[63]

In addition, NPs can act as physical shields for bacterial surfaces from Cr^{6+}, which could reduce the direct damage to bacteria caused by heavy metals. Encapsulating *S. loihica* by biochar reported that it could avoid the lethal effect of Cr^{6+}.[63] In addition, $Mn_{0.2}Fe_{2.8}O_4$ NPs can sustain bacterial viability, as shown in Fig. S1† and supported by the literature.[64] The Mn content in the chemical structure of $Mn_{0.2}Fe_{2.8}O_4$ NPs improved the anti-oxidant activity of NPs and, in turn, cell viability.[65] Substituting Fe^{2+} by Mn^{2+} in $Mn_{0.2}Fe_{2.8}O_4$ NPs decreased the lethal effect of Fe^{2+} on bacterial viability. This explains how $Mn_{0.2}Fe_{2.8}O_4$ NPs improved the viability of *S. oneidensis* MR-1 under the sub-lethal concentration of Cr^{6+} by 3.3 times.[23]

3.4 Boosting the bacterial tolerance to Cr^{6+} by $Mn_{0.2}Fe_{2.8}O_4$ NPs

SEM imaging monitored the alterations in the morphology of bacterial cells following the bio-reduction.

3.4.1 Morphology of untreated bacterial cells.
The untreated tested *S. oneidensis* MR-1 demonstrated their viability under anaerobic redox conditions, as shown in Fig. 4A. In the absence of both Cr^{6+} and $Mn_{0.2}Fe_{2.8}O_4$ NPs, bacterial cells of *S. oneidensis* MR-1 were observed as rod-shaped with smooth surfaces as commonly described.[22,49,63,66–68] The formation of the division ring (Z-ring) at the division site at the mid-cell on the bacteria was an indicator of cell division, as depicted in Fig. 4A. Parker *et al.*[22] reported that the delay in separating daughter cells could be ascribed to the minimum availability of nutrients in the media.[22] The presence of bacterial nanofibers as extensions of the outer membrane and periplasm (Fig. 4A) was demonstrated to be increased under oxygen-limited conditions.[66] Nanofibers were reported to have the multiheme cytochromes responsible for the extracellular electron transport pathway for linking the respiratory chain of bacteria to an external electron acceptor.[66] Electrons are transferred along nanofibers of *S. oneidensis* MR-1 between the close cytochromes *via* an electron-hopping mechanism.[67,68]

3.4.2 Rupture of *S. oneidensis* MR-1 cells in response to a sub-lethal dose of Cr^{6+}.
The impact of exposure of *S. oneidensis* MR-1 to Cr^{6+} was observed on the rupture on one pole of a cell, as shown in Fig. 4B. A shrunken surface and crack formation in bacteria cells were also observed after the reaction with Cr^{6+}.[22,49,69] As in the case of untreated cells, attempts of cell division were still observed for cells exposed to Cr^{6+}, as demonstrated in Fig. 4B. The presence of cell division septa was an indicator for the initial phase of cell division of *S. oneidensis* cells.[22] SEM images of *S. oneidensis* MR-1 revealed the inability to produce nanofibers after exposure to Cr^{6+}. The variation in the length of cells exposed to Cr^{3+} is presented in Fig. 4B. Bacterial cells modified their shape as a coping strategy for tolerating the stress induced by Cr^{6+}.[55,63]

3.4.3 Cellular compatibility of $Mn_{0.2}Fe_{2.8}O_4$ NPs.
Fig. S1† shows the biocompatibility of different concentrations of $Mn_{0.2}Fe_{2.8}O_4$ NPs towards *S. oneidensis* MR-1. Our findings were supported by Desai *et al.*, who reported that $MnFe_2O_4$ NPs showed no antimicrobial activity against some pathogenic bacteria.[70] *Shewanella* can survive upon exposure to 50 mg mL^{-1} of magnetite (Fe_3O_4) with approximately 36.2 mg mL^{-1} of total iron content under anaerobic conditions. Such tolerance to high iron concentrations was due to the cellular attachment to magnetite for Fe^{3+} acquisition.[71] The tolerance of *S. oneidensis* MR-1 to such concentrations of $Mn_{0.2}Fe_{2.8}O_4$ NPs could be attributed to the presence of Mn^{2+} in the chemical structure of NPs, which improved the antioxidant activity, cell viability, and ability to respire metal.[65] In addition, the Mn^{2+} content in $Mn_{0.2}Fe_{2.8}O_4$ NPs lowered Fe^{2+} concentration, which could decrease the lethal effect of Fe^{2+} on the viability of the tested bacterial strain. The presence of Fe^{3+} in $Mn_{0.2}Fe_{2.8}O_4$ NPs[23] has less toxicity than Fe^{2+} under physiological conditions.[72] The resistance of *S. oneidensis* MR-1 to Fe^{2+} depends on the ClpXP protease complex, which removes the mis-metallated protein. ClpX is an unfoldase, and ClpP is a peptidase that degrades damaged or misfolded proteins.[73]

The capability of *Shewanella* to produce nanofibers in the presence of $Mn_{0.2}Fe_{2.8}O_4$ NPs is shown in Fig. 4C. The poles of *Shewanella* cells were reported to be attractive to the metal oxide/hydroxides under both aerobic and anaerobic conditions,[74,75] which explains the polar rupture of some cells in Fig. 4C.

3.4.4 Enhanced tolerance of Shewanella to Cr^{6+} by $Mn_{0.2}Fe_{2.8}O_4$ NPs.
In the presence of $Mn_{0.2}Fe_{2.8}O_4$ NPs, the surface of the treated *S. oneidensis* MR-1 cells by Cr^{6+} retained a smooth surface but with an elongated morphology (see Fig. 4D). Such stretching in the shapes of cells was observed by *S. loihica* PV-4 in response to Cr^{6+} in a mixture containing biochar and α-Fe_2O_3 together.[63] The morphological changes observed in the bacteria are adaptive strategies for coping with environmental stresses like the presence of toxic Cr^{6+}. Inhibiting cell division while maintaining cell growth leads to increased cell length[76] and boosts the extracellular electron transfer by *S. oneidensis* MR-1.[77]
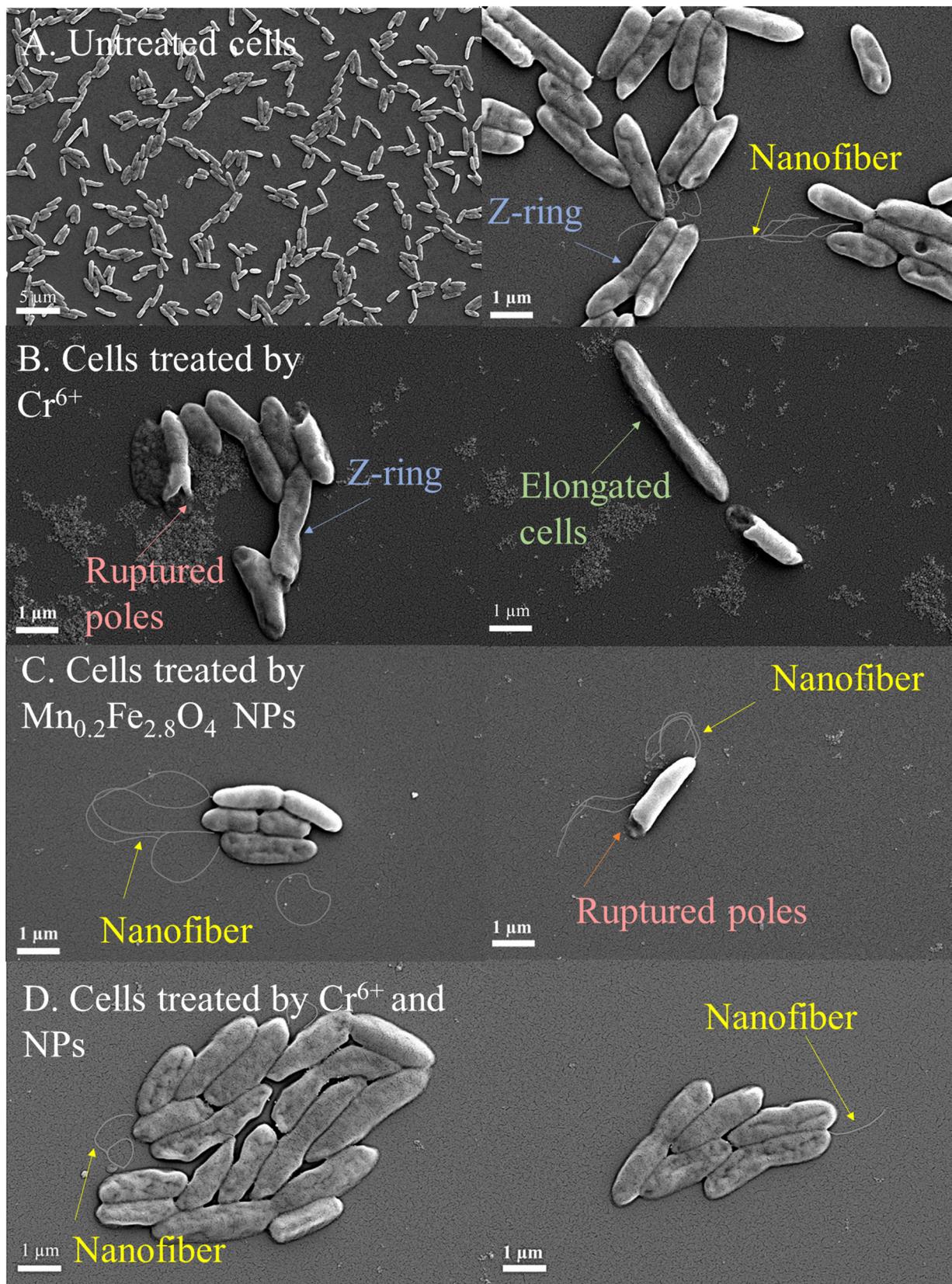
Fig. 4 SEM micrographs of (A) untreated *S. oneidensis* MR-1 cells, (B & C) treated cells by Cr^{6+} alone and NPs alone, respectively, and (D) treated cells by both Cr^{6+} and NPs.

This journal is © The Royal Society of Chemistry 2025

Environ. Sci.: Nano, 2025, **12**, 3035–3046 | **3041**

$Mn_{0.2}Fe_{2.8}O_4$ NPs provoked the formation of bacterial nanofiber in the presence of Cr^{6+}, as depicted in Fig. 4D. Nanofibers are extensions of the outer membrane and periplasm, which are the extracellular electron transport components.[66] Nanofibers are important for long-range extracellular electron transfer.[53,66] The ability of NPs to regenerate bacterial nanofiber production agrees with the findings reported by Yu *et al.*[53] Such observation in response to the interaction between $Mn_xFe_{3-x}O_4$ NPs and cells was confirmed in the present work by electron microscopy.

So, Fig. 5 summarises the protective role of $Mn_{0.2}Fe_{2.8}O_4$ NPs to *S. oneidensis* MR-1 bacterial cells during Cr^{6+}. The use of $Mn_{0.2}Fe_{2.8}O_4$ NPs improved the viability of *S. oneidensis* MR-1 under a sub-lethal concentration of Cr^{6+} by 3.3 times, as shown in our previous report.[23] Employing $Mn_{0.2}Fe_{2.8}O_4$ NPs as the adsorbent can limit the availability of Cr^{6+} to *S. oneidensis* MR-1, boosting the tolerance to Cr^{6+}.[18,69] The positive adsorptive effect of NPs on Cr^{6+} concerning the viability of bacteria has been reported in the presence of goethite, humic acid,[34] and ferric oxyhydroxide mediators.[18,69] As reported in our recent investigation,[23] Cr^{6+} was adsorbed on $Mn_{0.2}Fe_{2.8}O_4$ NPs following the Langmuir adsorption isotherm model. Based on this model, the adsorption and desorption rates should be equal. Adsorption is the separation of molecules from the aqueous solution by being attached to the surface of the adsorbent. The desorption is inversely related to adsorption processes, where adsorbates are transferred from the adsorbed state to bulk solution.[78] This possible continuous adsorption–desorption rate of Cr^{6+} can sustain a release of Cr^{6+} from the surface of NPs, which makes the exposure of cells to Cr^{6+} occur at a gradual rate.

Furthermore, $Mn_{0.2}Fe_{2.8}O_4$ NPs reduce Cr^{6+} into Cr^{3+}, as shown in Fig. 3B. Cr^{3+} is less toxic than Cr^{6+} towards *S. oneidensis* MR-1.[22] Bacterial cells exposed to Cr^{3+} experienced viability loss but maintained some enzymatic activity and cellular integrity,[22] which explains the morphological response of *S. oneidensis* MR-1 to Cr^{6+} in the presence of $Mn_{0.2}Fe_{2.8}O_4$ NPs, as shown in Fig. 4B.

4. Conclusion

This study describes a possible protecting role of manganese ferrite nanoparticles ($Mn_{0.2}Fe_{2.8}O_4$ NPs) to *Shewanella oneidensis* (*S. oneidensis*) MR-1 during hexavalent chromium (Cr^{6+}) bio-reduction. $Mn_{0.2}Fe_{2.8}O_4$ NPs can reduce the highly toxic Cr^{6+} to less toxic Cr^{3+}. Under anaerobic conditions, we found that $Mn_{0.2}Fe_{2.8}O_4$ NPs induced the elongation of the bacterial cells and promoted the formation of nanofibers. Such morphological change could improve the viability of *S. oneidensis* MR-1 cells in response to the sub-lethal dose of Cr^{6+} and, in turn, enhance
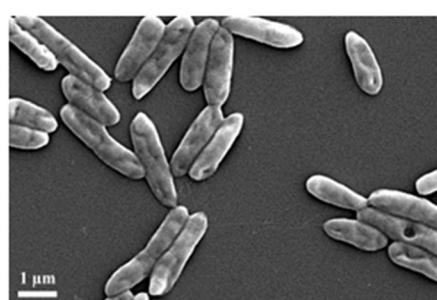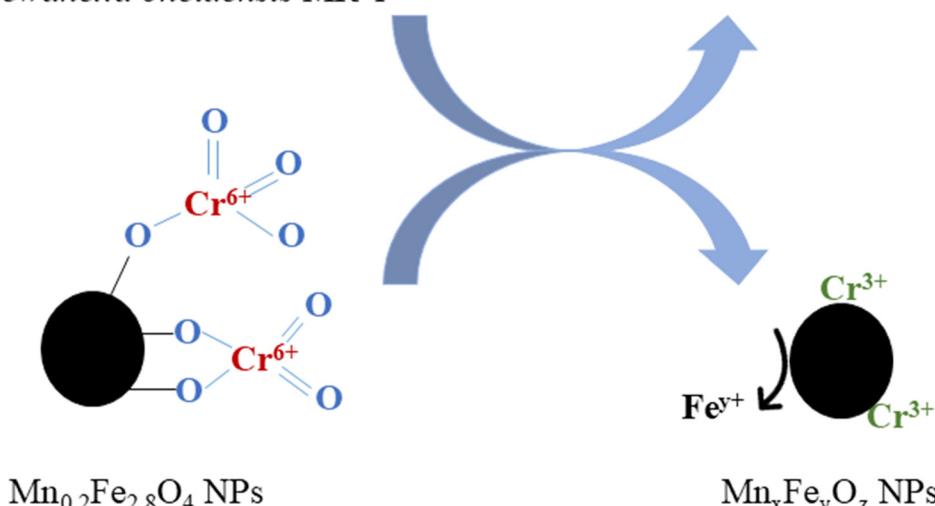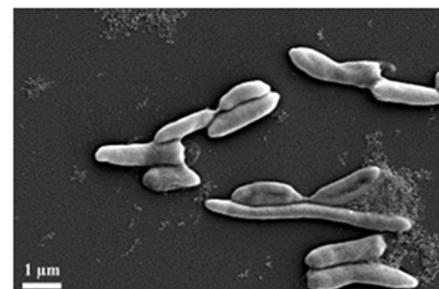
**Fig. 5** Illustration of the protective role of $Mn_{0.2}Fe_{2.8}O_4$ NPs to *S. oneidensis* MR-1 during $[CrO_4]^{2-}$ bio-reduction.

their detoxification ability. Integrating both *S. oneidensis* MR-1 and $Mn_{0.2}Fe_{2.8}O_4$ NPs enhanced Cr^{6+} detoxification by 2.1-fold compared to *S. oneidensis* MR-1 alone and 1.4-fold compared to NPs alone. Therefore, the present article provides evidence of Cr^{6+} bio-reduction and the bacterial response to Cr^{6+} and $Mn_{0.2}$-$Fe_{2.8}O_4$ NPs. This study will open a venue for applying nanotechnology in the bio-remediation of highly contaminated sites by heavy metals.

Data availability

The data within this study is included in either the main article or ESI† figures.

Author contributions

N. T. K. T. and L. C. devised and coordinated the project and provided resources. D. S. R. designed and did most of the experiments and wrote the manuscript. I. T. assisted in particle synthesis and data analysis. N. T. K. T. and S. M. provided expertise, revised the manuscript and helped to acquire funding. E. D. carried out XPS characterisation, processed data and corrected the manuscript. A. M. did a part of the characterisation and edited the manuscript.

Conflicts of interest

The authors declare no competing financial interest.

Acknowledgements

References

1 A. Monga, A. B. Fulke and D. Dasgupta, Recent developments in essentiality of trivalent chromium and toxicity of hexavalent chromium: Implications on human health and remediation strategies, *J. Hazard. Mater. Adv.*, 2022, **7**, 100113, Available from: https://www.sciencedirect.com/science/article/pii/S2772416622000699.

2 B. Pushkar, P. Sevak, S. Parab and N. Nilkanth, Chromium pollution and its bioremediation mechanisms in bacteria: A review, *J. Environ. Manage.*, 2021, **287**(February), 112279, DOI: 10.1016/j.jenvman.2021.112279.

3 E. Vaiopoulou and P. Gikas, Regulations for chromium emissions to the aquatic environment in Europe and elsewhere, *Chemosphere*, 2020, **254**, 126876, DOI: 10.1016/j.chemosphere.2020.126876.

4 T. L. Desmarias and M. Costa, Toxicology Mechanisms of chromium-induced toxicity, *Curr. Opin. Toxicol.*, 2019, **14**, 1–7, DOI: 10.1016/j.cotox.2019.05.003.

5 J. P. Wise, J. L. Young, J. Cai and L. Cai, Current understanding of hexavalent chromium [Cr(VI)] neurotoxicity and new perspectives, *Environ. Int.*, 2022, **158**, 106877, DOI: 10.1016/j.envint.2021.106877.

6 International Agency for Research on Cancer, List of Classifications–IARC Monographs on the Identification of Carcinogenic Hazards to Humans, Agents classified by the IARC Monographs, 2025, vol. 1–138, Available from: https://monographs.iarc.who.int/agents-classified-by-the-iarc/.

7 I. V. Y. Moffat, N. Martinova, C. Seidel and C. M. Thompson, Hexavalent Chromium in Drinking Water, *J. - Am. Water Works Assoc.*, 2018, **110**(5), E22–E35, DOI: 10.1002/awwa.1044.

8 European Parliament and the Council of the European Union, Directive (EU) 2020/2184 of the council of 16 December 2020 on the quality of water intended for human consumption (recast), *Official Journal of the European Union*, 2020, **435**(December), 1–62, Available from: https://eur-lex.europa.eu/eli/dir/2020/2184/oj/eng.

9 A. Rai, N. Kumar Sharma, V. Kumar Singh, A. Rai, V. Kumar and A. Kumar, *et al.*, Use of biowaste to ameliorate chromium-contaminated soils to improve crop productivity, *Waste Manag. Bull.*, 2024, **2**(1), 276–288, DOI: 10.1016/j.wmb.2024.02.004.

10 L. Li, Q. Liao, B. Hou, C. He, J. Liu and B. Li, *et al.*, Synchronous reduction and removal of hexavalent chromium from wastewater by modified magnetic chitosan beads, *Sep. Purif. Technol.*, 2023, **304**, 122363, Available from: https://www.sciencedirect.com/science/article/abs/pii/S1383586622019189.

11 J. Ding, Y. Guo, M. Tang and S. Zhou, Effects of exogenous riboflavin or cytochrome addition on the cathodic reduction of Cr (VI) in microbial fuel cell with Shewanella putrefaciens, *Environ. Sci. Pollut. Res.*, 2024, **31**(20), 29185–29198, Available from: https://link.springer.com/article/10.1007/s11356-024-33118-y.

12 L. J. Liermann, E. M. Hausrath, A. D. Anbar and S. L. Brantley, Assimilatory and dissimilatory processes of microorganisms affecting metals in the environment, *J. Anal. At. Spectrom.*, 2007, **22**(8), 867–877, Available from: https://pubs.rsc.org/en/content/articlelanding/2007/ja/b705383e/unauth.

13 J. Chen and Y. Tian, Hexavalent chromium reducing bacteria: mechanism of reduction and characteristics, *Environ. Sci. Pollut. Res.*, 2021, **28**(17), 20981–20997, DOI: 10.1007/s11356-021-13325-7.

14 M. Naveenkumar and K. Senthilkumar, Biomass and Bioenergy Microbial fuel cell for harvesting bio-energy from tannery effluent using metal mixed biochar electrodes, *Biomass Bioenergy*, 2021, **149**, 106082, DOI: 10.1016/j.biombioe.2021.106082.

This journal is © The Royal Society of Chemistry 2025

Environ. Sci.: Nano, 2025, **12**, 3035–3046 | **3043**

15 H. Gang, C. Xiao, Y. Xiao, W. Yan, R. Bai and R. Ding, *et al.*, Proteomic analysis of the reduction and resistance mechanisms of *Shewanella oneidensis* MR-1 under long-term hexavalent chromium stress, *Environ. Int.*, 2019, **127**, 94–102, DOI: **10.1016/j.envint.2019.03.016**.

16 R. Han, F. Li, T. Liu, X. Li, Y. Wu and Y. Wang, *et al.* Effects of incubation conditions on Cr(VI) reduction by c-type cytochromes in intact *Shewanella oneidensis* MR-1 cells, *Front. microbiol.*, 2016, **7**(MAY), 746, DOI: **10.3389/fmicb.2016.00746/full**.

17 Y. Yin, C. Liu, G. Zhao and Y. Chen, Versatile mechanisms and enhanced strategies of pollutants removal mediated by *Shewanella oneidensis*: A review, *J. Hazard. Mater.*, 2022, **440**, 165187–165211, DOI: **10.1016/j.jhazmat.2022.129703**.

18 X. Liu, G. Chu, Y. Du, J. Li and Y. Si, The role of electron shuttle enhances Fe(III)-mediated reduction of Cr(VI) by Shewanella oneidensis MR-1, *World J. Microbiol. Biotechnol.*, 2019, **35**(4), 64, DOI: **10.1007/s11274-019-2634-9**.

19 A. Elahi and A. Rehman, Multiple metal resistance and Cr^{6+} reduction by bacterium, *Staphylococcus sciuri* A-HS1, isolated from untreated tannery effluent, *J. King Saud Univ., Sci.*, 2019, **31**(4), 1005–1013, DOI: **10.1016/j.jksus.2018.07.016**.

20 S. Qin, W. Xiao, C. Zhou, Q. Pu, X. Deng and L. Lan, *et al. Pseudomonas aeruginosa*: pathogenesis, virulence factors, antibiotic resistance, interaction with host, technology advances and emerging therapeutics, *Signal Transduction Targeted Ther.*, 2022, **7**(1), 199, Available from: **https://www.nature.com/articles/s41392-022-01056-1**.

21 F. Mat Arisah, A. F. Amir, N. Ramli, H. Ariffin, T. Maeda and M. A. Hassan, *et al.* Bacterial resistance against heavy metals in *Pseudomonas aeruginosa* RW9 involving hexavalent chromium removal, *Sustainability*, 2021, **13**(17), 9797, Available from: **https://www.mdpi.com/2071-1050/13/17/9797**.

22 D. L. Parker, P. Borer and R. Bernier-Latmani, The response of *Shewanella oneidensis* MR-1 to Cr(III) toxicity differs from that to Cr(VI), *Front. microbiol.*, 2011, **2**(NOV), 223, DOI: **10.3389/fmicb.2011.00223/full**.

23 D. S. Raie, I. Tsonas, M. Canales, S. Mourdikoudis, K. Simeonidis and A. Makridis, *et al.*, Enhanced detoxification of Cr^{6+} by *Shewanella oneidensis* via adsorption on spherical and flower-like manganese ferrite nanostructures, *Nanoscale Adv.*, 2023, **5**(11), 2897–2910, Available from: **https://pubs.rsc.org/en/content/articlelanding/2023/na/d2na00691j**.

24 X. Lasheras, M. Insausti, J. M. De La Fuente, I. Gil De Muro, I. Castellanos-Rubio and L. Marcano, *et al.* Mn-Doping level dependence on the magnetic response of Mn$_x$Fe$_{3-x}$O$_4$ ferrite nanoparticles, *Dalton Trans.*, 2019, **48**(30), 11480–11491, Available from: **https://pubs.rsc.org/en/content/articlelanding/2019/dt/c9dt01620a**.

25 K. Vamvakidis, M. Katsikini, G. Vourlias, M. Angelakeris, E. C. Paloura and C. Dendrinou-Samara, Composition and hydrophilicity control of Mn-doped ferrite (Mn$_x$Fe$_{3-x}$O$_4$) nanoparticles induced by polyol differentiation, *Dalton Trans.*, 2015, **44**(12), 5396–5406, Available from: **https://pubs.rsc.org/en/content/articlelanding/2015/dt/c5dt00212e**.

26 O. Antonoglou and C. Dendrinou-Samara, Polyols as a Toolbox for the Preparation of Inorganic-based Nanostructures. in *Reducing Agents in Colloidal Nanoparticle Synthesis*, 2021, pp. 51–72, Available from: **https://books.rsc.org/books/edited-volume/912/chapter-abstract/708590/Polyols-as-a-Toolbox-for-the-Preparation-of?redirectedFrom=fulltext**.

27 N. T. K. Thanh, N. Maclean and S. Mahiddine, Mechanisms of nucleation and growth of nanoparticles in solution, *Chem. Rev.*, 2014, **114**(15), 7610–7630, DOI: **10.1021/cr400544s**.

28 H. H. Hau, A. Gilbert, D. Coursolle and J. A. Gralnick, Mechanism and consequences of anaerobic respiration of cobalt by *Shewanella oneidensis* strain MR-1, *Appl. Environ. Microbiol.*, 2008, **74**(22), 6880–6886, DOI: **10.1128/aem.00840-08**.

29 A. G. Shard, Practical guides for x-ray photoelectron spectroscopy: Quantitative XPS, *J. Vac. Sci. Technol., A*, 2020, **38**(4), 041201, Available from: **https://pubs.aip.org/avs/jva/article/38/4/041201/246897/Practical-guides-for-x-ray-photoelectron**.

30 D. García-Soriano, R. Amaro, N. Lafuente-Gómez, P. Milán-Rois, Á. Somoza and C. Navío, *et al.*, The influence of cation incorporation and leaching in the properties of Mn-doped nanoparticles for biomedical applications, *J. Colloid Interface Sci.*, 2020, **578**, 510–521, Available from: **https://www.sciencedirect.com/science/article/abs/pii/S002197972030758X**.

31 J. M. Hughes, P. M. Budd, A. Grieve, P. Dutta, K. Tiede and J. Lewis, Highly monodisperse, lanthanide-containing polystyrene nanoparticles as potential standard reference materials for environmental "nano" fate analysis, *J. Appl. Polym. Sci.*, 2015, **132**(24), 42061, DOI: **10.1002/app.42061**.

32 H. Etemadi and P. G. Plieger, Synthesis and characterisation of Mn$_x$Fe$_{3-x}$O$_4$ (M = Fe, Mn, Zn) spinel nanoferrites through a solvothermal route, *J. Mater. Sci.*, 2021, **56**(31), 17568–17583, DOI: **10.1007/s10853-021-06450-8**.

33 S. D. Oberdick, A. Abdelgawad, C. Moya, S. Mesbahi-Vasey, D. Kepaptsoglou and V. K. Lazarov, *et al.* Spin canting across core/shell Fe$_3$O$_4$/Mn$_x$Fe$_{3-x}$O$_4$ nanoparticles, *Sci. Rep.*, 2018, **8**(1), 3425, Available from: **https://www.nature.com/articles/s41598-018-21626-0**.

34 I. H. Fadhil Jasim, Thermal analysis and catalytic study of transition metals acetylacetonates, *Thermochim. Acta*, 1985, **93**, 65–68, Available from: **https://www.sciencedirect.com/science/article/abs/pii/0040603185850176**.

35 W. Shen, Z. Yao, Z. Liu, M. Xiao, J. Zhang and X. Zhang, *et al.*, The effect of dissolved oxygen and ultrasonic pretreatment on the Cr(VI) removal efficiency with manganese ferrite, *Desalin. Water Treat.*, 2022, **268**, 48–56, Available from: **https://www.sciencedirect.com/science/article/pii/S1944398624111319**.

36 I. Desai, M. N. Nadagouda, M. Elovitz, M. Mills and B. Boulanger, Synthesis and characterization of magnetic manganese ferrites, *Mater. Sci. Energy Technol.*, 2019, **2**(2), 150–160, DOI: **10.1016/j.mset.2019.01.009**.

37 J. Hu, I. M. C. Lo and G. Chen, Fast removal and recovery of Cr(VI) using surface-modified jacobsite (MnFe$_2$O$_4$) nanoparticles, *Langmuir*, 2005, **21**(24), 11173–11179, DOI: **10.1021/la051076h**.

3044 | *Environ. Sci.: Nano*, 2025, **12**, 3035–3046

This journal is © The Royal Society of Chemistry 2025

38 M. C. Biesinger, B. P. Payne, A. P. Grosvenor, L. W. M. Lau, A. R. Gerson and R. S. C. Smart, Resolving surface chemical states in XPS analysis of first row transition metals, oxides and hydroxides: Cr, Mn, Fe, Co and Ni, *Appl. Surf. Sci.*, 2011, **257**(7), 2717–2730, DOI: **10.1016/j.apsusc.2010.10.051**.

39 Z. Zhang, Y. Wang, Q. Tan, Z. Zhong and F. Su, Facile solvothermal synthesis of mesoporous manganese ferrite ($MnFe_2O_4$) microspheres as anode materials for lithium-ion batteries, *J. Colloid Interface Sci.*, 2013, **398**, 185–192, DOI: **10.1016/j.jcis.2013.01.067**.

40 T. Yamashita and P. Hayes, Analysis of XPS spectra of Fe^{2+} and Fe^{3+} ions in oxide materials, *Appl. Surf. Sci.*, 2008, **254**(8), 2441–2449, Available from: **https://www.sciencedirect.com/science/article/abs/pii/S0169433207013748**.

41 T. Radu, C. Iacovita, D. Benea and R. Turcu, X-Ray Photoelectron Spectroscopic Characterization of Iron Oxide Nanoparticles, *Appl. Surf. Sci.*, 2017, **405**, 337–343, DOI: **10.1016/j.apsusc.2017.02.002**.

42 B. P. Payne, M. C. Biesinger and N. S. McIntyre, X-ray photoelectron spectroscopy studies of reactions on chromium metal and chromium oxide surfaces, *J. Electron Spectrosc. Relat. Phenom.*, 2011, **184**(1–2), 29–37, Available from: **https://www.sciencedirect.com/science/article/abs/pii/S0368204810002586**.

43 K. Jagannathan, A. Srinivasan and C. N. R. Rao, An XPS study of the surface oxidation states of metals in some oxide catalysts, *J. Catal.*, 1981, **69**(2), 418–427, Available from: **https://www.sciencedirect.com/science/article/abs/pii/0021951781901779**.

44 R. Aymerich-Armengol, P. Cignoni, P. Ebbinghaus, J. Linnemann, M. Rabe and K. Tschulik, *et al.*, Mechanism of coupled phase/morphology transformation of 2D manganese oxides through Fe galvanic exchange reaction, *J. Mater. Chem. A*, 2022, **10**(45), 24190–24198, Available from: **https://pubs.rsc.org/en/content/articlelanding/2022/ta/d2ta06552e**.

45 J. Chwastowski, P. Staroń, H. Kołoczek and M. Banach, Adsorption of hexavalent chromium from aqueous solutions using Canadian peat and coconut fiber, *J. Mol. Liq.*, 2017, **248**, 981–989, Available from: **https://www.sciencedirect.com/science/article/abs/pii/S0167732217341120**.

46 X. Liu, H. Dong, X. Yang, L. Kovarik, Y. Chen and Q. Zeng, Effects of citrate on hexavalent chromium reduction by structural Fe(II) in nontronite, *J. Hazard. Mater.*, 2018, **343**, 245–254, Available from: **https://www.sciencedirect.com/science/article/abs/pii/S0304389417307288**.

47 B. Sarkar, R. Naidu, G. S. R. Krishnamurti and M. Megharaj, Manganese(II)-catalyzed and clay-minerals-mediated reduction of chromium(VI) by citrate, *Environ. Sci. Technol.*, 2013, **47**(23), 13629–13636, DOI: **10.1021/es401568k**.

48 A. Mohamed, B. Sun, C. Yu, X. Gu, N. Ashry and Y. Riahi, *et al.* Size effect of hematite particles on the Cr(VI) reduction by *Shewanella oneidensis* MR-1, *J. Environ. Chem. Eng.*, 2021, **9**(2), 105096, DOI: **10.1016/j.jece.2021.105096**.

49 C. Ri, J. Tang, F. Liu, H. Lyu and F. Li, Enhanced microbial reduction of aqueous hexavalent chromium by *Shewanella oneidensis* MR-1 with biochar as electron shuttle, *J. Environ. Chem. Eng.*, 2022, **113**, 12–25, DOI: **10.1016/j.jes.2021.05.023**.

50 R. Elmeihy, X. C. Shi, P. Ll Tremblay and T. Zhang, Fast removal of toxic hexavalent chromium from an aqueous solution by high-density *Geobacter sulfurreducens*, *Chemosphere*, 2021, **263**, 128281, DOI: **10.1016/j.chemosphere.2020.128281**.

51 J. Cheng, J. Gao, J. Zhang, W. Yuan, S. Yan and J. Zhou, *et al.*, Optimization of Hexavalent Chromium Biosorption by *Shewanella putrefaciens* Using the Box-Behnken Design, *Water, Air, Soil Pollut.*, 2021, **232**(3), 92, DOI: **10.1007/s11270-020-04947-7**.

52 Y. Xiao, C. Xiao and F. Zhao, Long-term adaptive evolution of *Shewanella oneidensis* MR-1 for establishment of high concentration Cr(VI) tolerance, *Front. Environ. Sci. Eng.*, 2020, **14**(1), 3, DOI: **10.1007/s11783-019-1182-8**.

53 C. Yu, L. Yu, A. Mohamed, J. Fang, Y. Wu and K. Dai, *et al.* Size-dependent visible-light-enhanced Cr(VI) bioreduction by hematite nanoparticles, *Chemosphere*, 2022, **295**(October 2021), 133633, Available from: **https://www.sciencedirect.com/science/article/abs/pii/S0045653522001266**.

54 H. Cheng, Z. Jing, L. Yang, A. Lu, G. Ren and J. Liu, Sunlight-triggered synergy of hematite and *Shewanella oneidensis* MR-1 in Cr(VI) removal, *Geochim. Cosmochim. Acta*, 2021, **305**, 19–32, DOI: **10.1016/j.gca.2021.04.034**.

55 G. Wang, B. Zhang, S. Li, M. Yang and C. Yin, Simultaneous microbial reduction of vanadium (V) and chromium (VI) by *Shewanella loihica* PV-4, *Bioresour. Technol.*, 2017, **227**, 353–358, DOI: **10.1016/j.biortech.2016.12.070**.

56 L. Ma, Y. Du, S. Chen, F. Zhang, W. Zhan and D. Du, *et al.*, Nanoscale zero-valent iron coupling with *Shewanella oneidensis* MR-1 for enhanced reduction/removal of aqueous Cr(VI), *Sep. Purif. Technol.*, 2021, **277**(August), 119488, DOI: **10.1016/j.seppur.2021.119488**.

57 L. Liu, J. Zhao, W. Yin, S. Lv, M. Su and P. Li, *et al.*, Enhanced immobilization of Cr(VI) by a Fe^0–microorganisms composite system: Benchmark and pot experiments, *J. Environ. Qua*, 2021, **50**(5), 1123–1134, DOI: **10.1002/jeq2.20261**.

58 L. Ma, Y. Du, S. Chen, D. Du, H. Ye and T. C. Zhang, Highly efficient removal of Cr(VI) from aqueous solution by pinecone biochar supported nanoscale zero-valent iron coupling with *Shewanella oneidensis* MR-1, *Chemosphere*, 2022, **287**(P2), 132184, DOI: **10.1016/j.chemosphere.2021.132184**.

59 Y. Ma, X. Wu, Z. Shi, X. Li, S. Qian and X. Sun, *et al.* Photoactive Manganese Ferrite-Modified Bacterial Anode to Simultaneously Boost Both Mediated and Direct Electron Transfer Processes in Microbial Fuel Cells, *ACS Sustainable Chem. Eng.*, 2022, **10**(10), 3355–3362, DOI: **10.1021/acssuschemeng.1c08683**.

60 J. Ifthikar, I. I. Shahib, A. Jawad, E. A. Gendy, S. Wang and B. Wu, *et al.*, The excursion covered for the elimination of chromate by exploring the coordination mechanisms between chromium species and various functional groups, *Coord. Chem. Rev.*, 2021, **437**, 213868, Available from: **https://www.sciencedirect.com/science/article/abs/pii/S0010854521001028**.

61 M. Lu, Z. Su, Y. Zhang, H. Zhang, J. Wang and Q. Li, *et al.* Mn-Doped Spinel for Removing Cr(VI) from Aqueous Solutions: Adsorption Characteristics and Mechanisms, *Materials*, 2023, **16**(4), 1553, Available from: **https://www.mdpi.com/1996-1944/16/4/1553**.

62 S. Khilari, S. Pandit, J. L. Varanasi, D. Das and D. Pradhan, Bifunctional Manganese Ferrite/Polyaniline Hybrid as Electrode Material for Enhanced Energy Recovery in Microbial Fuel Cell, *ACS Appl. Mater. Interfaces*, 2015, **7**(37), 20657–20666, DOI: **10.1021/acsami.5b05273**.

63 D. Zou, J. Tong, C. Feng, Y. Wang, X. Li and X. Zheng, *et al.*, Synthesis of biochar@α-Fe$_2$O$_3$@*Shewanella loihica* complex for remediation of soil contaminated by hexavalent chromium: optimization of conditions and mechanism, *Chemosphere*, 2022, **303**, 134858, Available from: **https://www.sciencedirect.com/science/article/abs/pii/S0045653522013510**.

64 C. R. Myers and K. H. Nealson, Bacterial manganese reduction and growth with manganese oxide as the sole electron acceptor, *Dhaka Univ. Stud., Part B*, 1988, **240**(4857), 1319–1321, DOI: **10.1126/science.240.4857.1319**.

65 I. L. Gunsolus, M. N. Hang, N. V. Hudson-Smith, J. T. Buchman, J. W. Bennett and D. Conroy, *et al.*, Influence of nickel manganese cobalt oxide nanoparticle composition on toxicity toward *Shewanella oneidensis* MR-1: redesigning for reduced biological impact, *Environ. Sci.:Nano*, 2017, **4**(3), 636–646, Available from: **https://pubs.rsc.org/en/content/articlelanding/2017/en/c6en00453a**.

66 S. Pirbadian, S. E. Barchinger, K. M. Leung, H. S. Byun, Y. Jangir and R. A. Bouhenni, *et al.*, *Shewanella oneidensis* MR-1 nanowires are outer membrane and periplasmic extensions of the extracellular electron transport components, *Proc. Natl. Acad. Sci. U. S. A.*, 2014, **111**(35), 12883–12888, DOI: **10.1073/pnas.1410551111**.

67 N. S. Malvankar and D. R. Lovley, Microbial nanowires for bioenergy applications, *Curr. Opin. Biotechnol.*, 2014, **27**, 88–95, DOI: **10.1016/j.copbio.2013.12.003**.

68 P. Subramanian, S. Pirbadian, M. Y. El-Naggar and G. J. Jensen, Ultrastructure of *Shewanella oneidensis* MR-1 nanowires revealed by electron cryotomography, *Proc. Natl. Acad. Sci. U. S. A.*, 2018, **115**(14), E3246–E3255, DOI: **10.1073/pnas.1718810115**.

69 A. Mohamed, L. Yu, Y. Fang, N. Ashry, Y. Riahi and I. Uddin, *et al.* Iron mineral-humic acid complex enhanced Cr(VI) reduction by *Shewanella oneidensis* MR-1, *Chemosphere*, 2020, **247**, 125902, Available from: **https://www.sciencedirect.com/science/article/abs/pii/S0045653520300941**.

70 H. B. Desai, S. Ghosh, R. Pandit and A. R. Tanna, Synergistic bacteriostatic effect of streptomycin-coated nanomagnetic functional oxides, *BioNanoScience*, 2021, **12**, 62–73, DOI: **10.1007/s12668-021-00923-5**.

71 J. A. Roberts, D. A. Fowle, B. T. Hughes and E. Kulczycki, Attachment behavior of *Shewanella putrefaciens* onto magnetite under aerobic and anaerobic conditions, *Geomicrobiol. J.*, 2006, **23**(8), 631–640, DOI: **10.1080/01490450600964441**.

72 B. D. Bennett and J. A. Gralnick, Mechanisms of toxicity by and resistance to ferrous iron in anaerobic systems, *Free Radical Biol. Med.*, 2019, **140**(June), 167–171, DOI: **10.1016/j.freeradbiomed.2019.06.027**.

73 B. D. Bennett, K. E. Redford and J. A. Gralnick, Survival of Anaerobic Fe^{2+} Stress Requires the ClpXP Protease, *J. Bacteriol.*, 2018, **200**(8), e00671-17, DOI: **10.1128/jb.00671-17**.

74 S. Glasauer, S. Langley and T. J. Beveridge, Sorption of Fe (Hydr)Oxides to the Surface of *Shewanella putrefaciens*: Cell-Bound Fine-Grained Minerals Are Not Always Formed de Novo, *Appl. Environ. Microbiol.*, 2001, **67**(12), 5544–5550, DOI: **10.1128/aem.67.12.5544-5550.2001**.

75 M. C. Grantham, P. M. Dove and T. J. DiChristina, Microbially catalyzed dissolution of iron and aluminum oxyhydroxide mineral surface coatings, *Geochim. Cosmochim. Acta*, 1997, **61**(21), 4467–4477, Available from: **https://www.sciencedirect.com/science/article/abs/pii/S0016703797002652**.

76 S. S. Justice, D. A. Hunstad, L. Cegelski and S. J. Hultgren, Morphological plasticity as a bacterial survival strategy, *Nat. Rev. Microbiol.*, 2008, **6**(2), 162–168, Available from: **https://www.nature.com/articles/nrmicro1820**.

77 F. Li, H. Yu, B. Zhang, C. Hu, F. Lan and Y. Wang, *et al.* Engineered Cell Elongation Promotes Extracellular Electron Transfer of *Shewanella Oneidensis*, *Adv. Sci.*, 2024, **11**(41), 2403067, DOI: **10.1002/advs.202403067**.

78 S. Azizian, S. Eris and L. D. Wilson, Re-evaluation of the century-old Langmuir isotherm for modeling adsorption phenomena in solution, *Chem. Phys.*, 2018, **513**, 99–104, Available from: **https://www.sciencedirect.com/science/article/abs/pii/S0301010418305317**.

3046 | *Environ. Sci.: Nano*, 2025, **12**, 3035–3046

This journal is © The Royal Society of Chemistry 2025